Aerodynamic Performance of a Hovering Microrotor in Confined Environment



Thierry Jardin
Research Scientist

Sebastien Prothin*
Research Scientist

Cristian García Magaña
M. Res. Student

Institut Supérieur de l'Aéronautique et de l'Espace (ISAE-SUPAERO), Université de Toulouse, Toulouse, France

This paper aims at understanding how the aerodynamic performance of a hovering microrotor is affected by horizontal and vertical wall proximity. Toward that end, experiments are performed to extract aerodynamic loads and velocity flow fields from strain gauges and high-definition stereoscopic particle image velocimetry measurements, respectively. The results show that horizontal wall boundary conditions contribute to enhancing aerodynamic performance, whereas vertical boundary conditions have a negligible impact. Enhancement of aerodynamic performance arises from distinct flow physics, such as rotor wake expansion or Venturi effects, that depend on the configuration considered. These results open the path toward the development of micro air vehicles dedicated to the exploration of highly confined environments.

Introduction

Micro air vehicles (MAVs) have recently gained interest owing to their ability to perform missions of observation at relatively low cost. In response to the 1996–2000 MAV Program initiative by the U.S. Defense Advanced Research Projects Agency (DARPA), three main concepts of MAVs have emerged: fixed-wing, rotary-wing, and flapping-wing MAVs (Refs. 1–3). Fixed-wing MAVs are mostly dedicated to long-range missions due to their relatively long-endurance and high-speed range. However, they are not hovering capable and are hence mostly restricted to outdoor missions. Conversely, rotary-wing MAVs suffer from low endurance but offer the possibility to evolve in confined environment due to their ability to perform hovering flight and to achieve enhanced maneuverability. While the two former concepts simply derive from the scaling of conventional aircraft and helicopters, the flapping-wing concept derives from the observation of nature. This alternative bioinspired concept could potentially allow hovering flight, enhanced maneuverability, and low noise generation while providing reasonable aerodynamic performance, hence endurance, at low Reynolds numbers typical of insect flight. Although flapping-wing MAVs may appear as a promising concept at several levels, they involve complex mechanical systems and complex aerodynamics that make it an immature technology (Refs. 4–7). Thus, to date, rotary-wing MAVs appear as the most relevant solution for missions of observation in confined environments.

While the aerodynamic performance of hovering microrotors in nonconfined environments has been extensivelystudied (Refs. 8–11), virtually no research work has focused on microrotors in highly confined environments. Few studies report results of microrotors in ground effect (IGE) though, showing that a rotor hovering in the vicinity of the ground outperforms a hovering rotor out-of-ground effect (OGE). These results are of paramount importance for both the design of efficient autopilot and the definition of low-consumption flight strategies (Ref. 12). In this context, Lee et al. and Lakshminarayan et al. (Refs. 13, 14) have brought to the fore the complexity of the flow that develops around an IGE microrotor using particle image velocimetry (PIV) measurements and URANS computations, respectively. Nathan and Green (Ref. 15) have experimentally investigated the flow around an IGE microrotor both hovering in crosswind and in forward flight. On the basis of PIV measurements, the authors have highlighted differences between the two configurations in the transition from recirculation regime to ground vortex regime. In another context, still using IGE microrotors, various authors motivated by the necessity to augment knowledge on the brownout phenomenon have unraveled the prominent flow features that promote upliftment of sediment particles (Refs. 16–18). Although only a few studies were reported for microrotors, relevant information on the main features of IGE flight can be transposed from extensive studies related to large-scale rotors (Refs. 19–23).

Overall, the aforementioned studies demonstrate that boundary conditions are critical to the aerodynamic performance of microrotors as they may significantly constrain the development of the rotor wake. In this paper, we extend previous works to the experimental analysis of lateral and upper wall effects, as well as channel and duct effects. These configurations modelize highly confined environments that may be encountered by an MAV performing indoor reconnaissance.

In particular, we show that ceiling effects have a beneficial impact on aerodynamic performance, in a rather similar way to that obtained in ground effects yet through a distinct physical mechanism. Furthermore,

*Corresponding author; e-mail: sebastien.prothin@isae.fr.

Part of this work was presented at the AHS 71st Annual Forum, Virginia Beach, VA, May 5–7, 2015. Manuscript received September 2015; accepted November 2016.

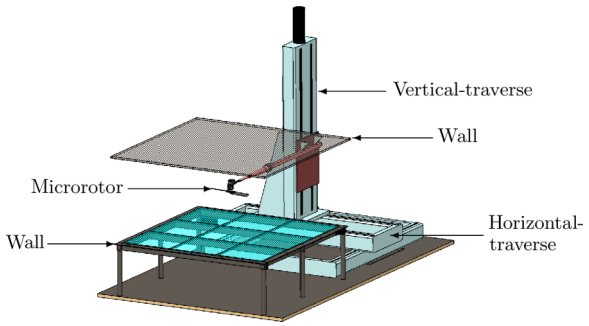

Fig. 1. Illustration of the experimental setup.

channel effects seem to derive from a simple linear combination of both ceiling and ground effects. In contrast, lateral walls have negligible effects on aerodynamic performance whether they are isolated or in duct configuration. All these observations help raise guidelines for the design of efficient autopilot.

Experimental Setup

An illustration of the experimental setup is shown in Fig. 1. The microrotor has a radius $R = 125$ mm and consists of two untwisted flat plates with constant pitch angle. Interchangeable hubs are manufactured that allow different pitch angles θ to be set in the range 5°–35°.

For each case, the rotor was powered using an AXI 2808/24 goldline brushless motor. A proportional–integral–derivative (PID) controller was implemented to operate the rotor at rotational frequencies ranging from 20 to 140 Hz within ±1% accuracy. Variations in rotational frequencies allowed to keep the rotor thrust constant for different rotor-to-boundaries distances.

The rotor was operated such that its tip–path plane was parallel and/or perpendicular to wall boundary conditions, depending on the configuration considered. It was connected via a 600-mm-long steel beam to a mechanical traverse that allowed automatic adjustment of the rotor-to-boundaries distance. Wall boundaries consisted of 900×900 mm^2 (roughly $7.2 \times 7.2\ R^2$) plexiglas (ground plane) and wooden (upper and side walls) plates.

The rotor was mounted on an offset ATI Nano 125 balance that allowed force and torque components to be measured within ±1% accuracy. The maximum range of the balance was 125 N and 3 Nm for force and torque measurements, respectively. Mean forces and torques were obtained by averaging 50,000 samples acquired at a frequency of 5 kHz over a time interval of 10 s. For relevant cases, four runs were performed to assess the repeatability of the load measurements. Moreover, data obtained with the motor-mounted upstream and downstream of the rotor (to allow small gaps between the rotor and the boundaries) were found to overlap within the error margin.

In addition, for the specific 15° pitch angle case, velocity flow fields in the axial plane of the rotor were obtained through high-definition stereoscopic PIV measurements. Two FlowSense EO 16M cameras were synchronized to a 2×200-mJ DualPower Bernoulli laser and driven via DynamicStudio (Dantec) commercial software. While the laser was operated at a nominal 15-Hz frequency, PIV images were acquired at 2.5 Hz (every six laser impulse) due to the maximum 2.6 Hz allowable operating frequency of the cameras. The laser power was set to 35 mJ to limit laser reflections on the rotor and the walls. The cameras were equipped with a 85-mm-focal-length Samyang lens, $F\#$ 4. A Jem ZR44 Hi-Mass fog generator was used to obtain a homogeneous seeding of water-based spherical particles in the entire volume enclosing the experimental setup. The seeding was such that approximately 10 particles were contained within one interrogation PIV window, with a particle being discretized into approximately five pixels. The time step between two images used for the cross-correlation was set to 80 μs. Velocities were computed using an adaptive cross-correlation (two refinement steps) with a final window size of 16×16 px^2, and spurious velocities were identified using a peak ratio validation procedure (with a peak-to-peak ratio of 1.2). Note that the mean percentage of rejected vectors was on the order of 2%. The final dimensions of the reconstructed three-component flow fields were approximately 600×400 mm^2 ($4.8 \times 3.8\ R^2$), leading to a spatial resolution of 0.25 mm ($2 \times 10^{-3}\ R$). For each case, 1000 instantaneous velocity flow fields were averaged, ensuring convergence of both mean and fluctuating values. In what follows, all velocities are nondimensionalized using the induced velocity v_i derived from rotor thrust measurement T and momentum theory: $v_i = \sqrt{T/2\rho\pi R^2}$.

Note that the specific 15° pitch angle case is chosen for PIV measurements because it is close to the maximum efficiency pitch angle. Recent numerical results on a similar geometry (Ref. 24) show that in this case, the flow separates at the leading edge and rolls up into a recirculation bubble (or leading edge vortex) that remains attached to the upper surface of the blade, thereby increasing the virtual camber of the blade profile. In addition, it is worth mentioning that blade element momentum theory predicts local effective incidences along the blade span lower than 10° for all rpm tested in this paper.

Results

This section aims at understanding how horizontal and lateral wall boundary conditions affect the aerodynamic performance of microrotors. Toward that end, we focus on the evolution of the power loading (PL) as a function of the nondimensional distance h/R that separates the center of the rotor disk from the wall, at a given disk loading (DL). Recall that PL is defined as the ratio between the thrust and the power of the rotor $T/Q\omega$, and that DL is defined as the ratio between the thrust and the area of the rotor disk T/A, with $A = \pi R^2$. The PL $= f(h/R)|_{\mathrm{DL}}$ curve is of paramount importance in practice as it reveals the enhancement or degradation of the aerodynamic performance of a given MAV as it approaches horizontal or lateral walls.

Ground effects

Figure 2 displays the evolution of the ratio of the PL obtained in and out-of-ground effects as a function of the rotor-to-ground distance h/R, at a given DL and for $\theta = 15°$. It is shown that $\mathrm{PL_{IGE}/PL_{OGE}}$ is roughly constant for values of h/R above 2 but rapidly increases for values of h/R below 2, as h/R tends to 0.

This trend, which is extensively reported in the literature, is associated with the radial expansion of the rotor jet. Such a phenomenon is illustrated in Fig. 3, which depicts streamlines and fluctuating radial velocity isolines superimposed on velocity magnitude isocontours for both $h/R = 1$ and 2 IGE cases.

Overall, it is shown that the rotor jet expands radially, away from the rotor axis where a strong recirculation region develops. In the $h/R = 2$ case, the recirculation region in the vicinity of the ground is sufficiently far away from the rotor disk to allow for a slight contraction of the jet immediately downstream of the rotor hub before the flow is constrained to circumvent the recirculation region in the outward direction. In the $h/R = 1$ case, the recirculation region is tilted along the rotor axis direction and fills the gap between the rotor and the ground, preventing any jet contraction. Here, the flow is severely constrained in the outward

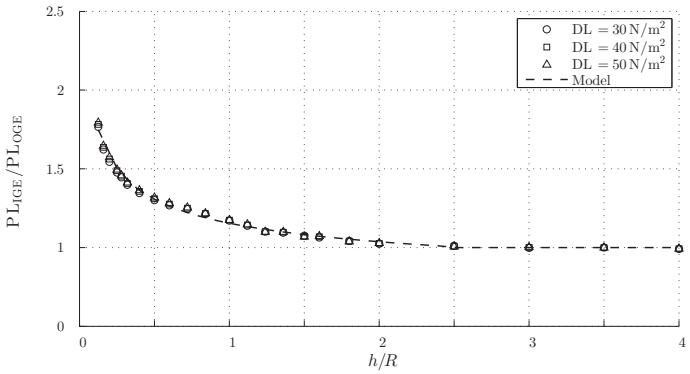

Fig. 2. PL_{IGE}/PL_{OGE} ratio as a function of the nondimensional rotor-to-ground distance h/R for $\theta = 15°$.

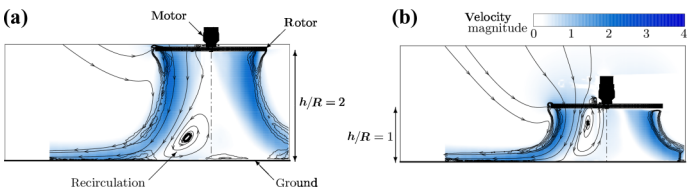

Fig. 3. Streamlines and isolines of radial fluctuating velocities superimposed on contours of velocity magnitude. Flow fields obtained for the $h/R = 2$ (a) and $h/R = 1$ (b) IGE configurations with $\theta = 15°$.

direction immediately after the rotor disk. This simple comparison between the $h/R = 1$ and 2 cases thus shows that the jet expansion is more pronounced for low values of h/R.

The influence of ground proximity on jet expansion is further highlighted in Fig. 4, which shows the periphery of the jet for different h/R cases. The periphery of the jet is here extracted from local maxima of radial velocity fluctuations. It clearly appears that jet expansion increases with decreasing values of h/R. In particular, it is shown that the area of the minimum jet section (i.e., where the radial contraction of the jet is the highest) obtained at a given h/R decreases from 0.78A at $h/R = 1$ to 0.61A at $h/R = 4$. In addition, such an expansion is correlated with a reduction and homogeneization of the axial velocity at the rotor disk. This is highlighted in Fig. 4, which depicts spanwise profiles of axial induced velocity at the rotor disk. This mechanism, together with a reduction in tip vortex strength, is known to promote aerodynamic efficiency (Ref. 21). Overall, three main features can be observed: (1) axial velocity along most of the blade span is reduced, (2) maximum axial velocity is reduced and moved toward the wing tip, and (3) negative velocities are induced at the blade root due to the interaction with the recirculation region.

The increase in PL_{IGE}/PL_{OGE} with decreasing h/R values can also be viewed as an increase in thrust at a given power. This extra lift when approaching the ground is appreciated by helicopter pilots as it contributes to secure landing phases. In the framework of MAVs, another interest emerges; that of significantly reducing power consumption and hence increasing flight endurance when flight is performed IGE. In other words, an interesting strategy to enhance MAVs endurance is to allow for robust IGE flight. This requires to promote flight robustness through the definition of simple models dedicated to autopilot design. As such, Fig. 2 shows that empirical asymptotic models of the form $a \times (h/R)^{-b} + c$, with $b = 0.36$ in this case, provide a reasonable estimate of the evolution of PL_{IGE}/PL_{OGE} as a function of h/R. Furthermore, it is interesting to

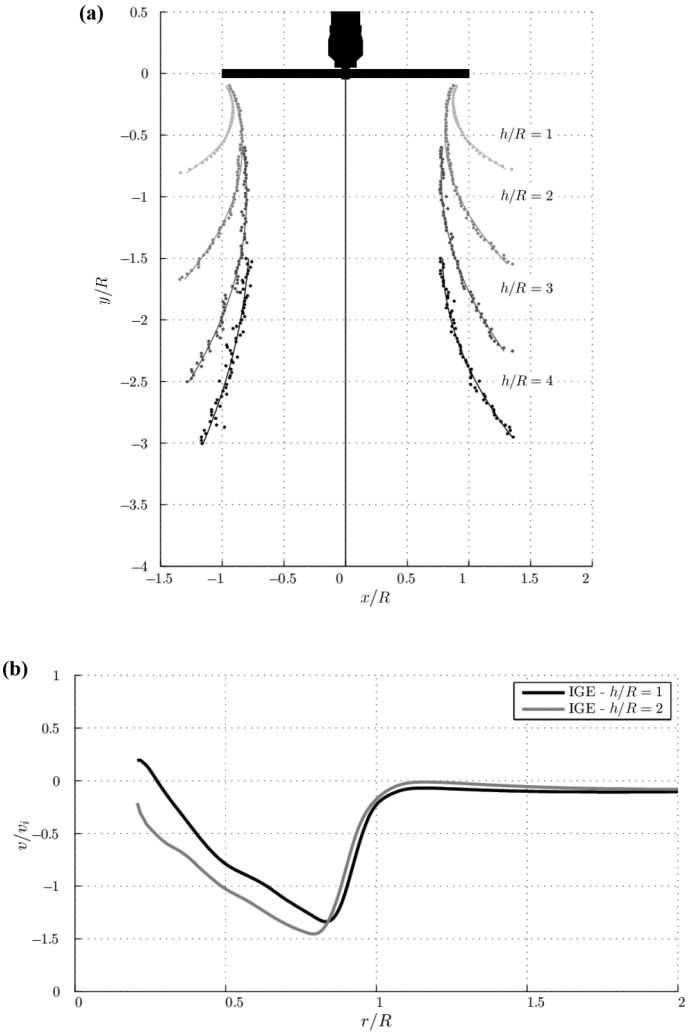

Fig. 4. Location of the rotor jet periphery deduced from local maxima of radial velocity fluctuations (a) and nondimensional axial velocity at the rotor disk (b) for the IGE configurations with $\theta = 15°$.

note that the evolution of PL_{IGE}/PL_{OGE}, and hence the model, is roughly independent of DL.

On the other hand, the evolution of PL_{IGE}/PL_{OGE} highly depends on the pitch angle. Figure 5 shows PL_{IGE}/PL_{OGE} as a function of the pitch angle θ for four values of $h/R = 0.125$, 0.6, 1, and 4. It can be observed that low pitch angle cases are more sensitive to ground proximity. Simple considerations on two-dimensional airfoil aerodynamics suggest that aerodynamic performance is more sensitive to changes in angle of attack when the latter is low. Therefore, a modification in effective incidence of the local blade profile, via a modification in local induced velocity, should have a more pronounced impact on blade profile efficiency at low incidence (i.e., low pitch angles) than it has at high incidence (i.e., high pitch angles). It is noteworthy to mention that while the strongest sensitivity of aerodynamic performance to changes in angle of attack is generally observed for values of angle of attack below 10° on two-dimensional airfoils, it can be pushed toward higher values for microrotors where nonnegligible three-dimensional effects may occur.

Data obtained for different pitch angles suggest that, as a first approach, the coefficients a and b of the asymptotic models $a \times (h/R)^{-b} + c$ can roughly be defined as linear and quadratic functions of θ, respectively.

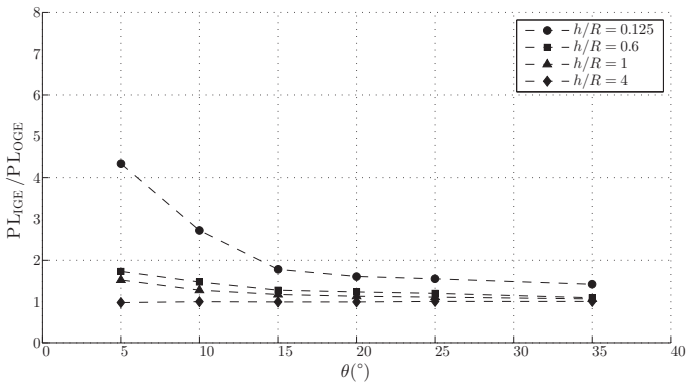

Fig. 5. $\mathrm{PL_{IGE}/PL_{OGE}}$ ratio as a function of pitch angle θ for different h/R values.

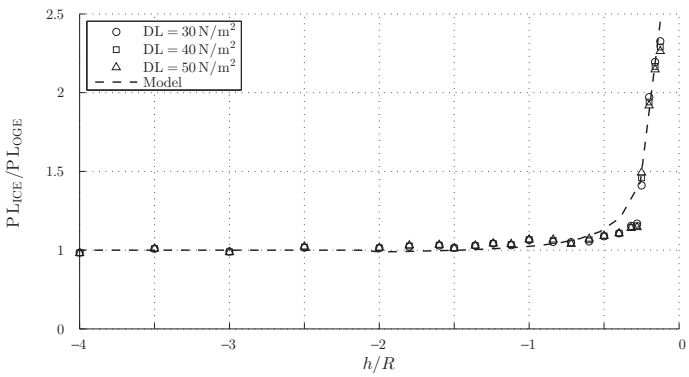

Fig. 6. $\mathrm{PL_{ICE}/PL_{OGE}}$ ratio as a function of the nondimensional rotor-to-ceiling distance h/R for $\theta = 15°$.

Ceiling effects

While it is known that MAVs endurance can significantly benefit from IGE flight phases, we here ask whether MAVs can benefit from flight phases in ceiling effects (ICE)? The literature on rotors being historically associated with the study of manned helicopters, and the latter are being not confronted to ICE flight phases in practice; this MAVs-specific flight configuration is virtually undocumented.

Similarly to the IGE case, Fig. 6 shows the evolution of the $\mathrm{PL_{ICE}/PL_{OGE}}$ ratio as a function of the rotor to ceiling distance h/R, at a given DL. A prominent feature is the drastic increase in $\mathrm{PL_{ICE}/PL_{OGE}}$ as h/R tends to 0. This increase is stronger than that observed in the IGE case, with values of $\mathrm{PL_{ICE}/PL_{OGE}}$ reaching 2.29 at $h/R = 0.125$ (to be compared with the value of 1.78 at $h/R = 0.12$ in the IGE case). Furthermore, ceiling effects occur at lower values of h/R than IGE effects and thus appear as a more sudden and severe phenomenon.

Conversely to the IGE case, the increase in $\mathrm{PL_{ICE}/PL_{OGE}}$ for decreasing values of h/R is not related to any jet expansion. Rather, the proximity of the ceiling restricts the axial incoming flow above the rotor, which is to be compensated by the development of a radial incoming flow. This feature is visible in Fig. 7, which depicts streamlines and fluctuating radial velocity isolines superimposed on velocity magnitude isocontours for both $h/R = 1$ and 2 ICE cases.

Furthermore, Fig. 8 shows that the proximity of the ceiling and the restriction in axial incoming flow above the rotor does not significantly alter the axial induced velocity at the rotor disk, despite a reduction in maximum axial velocity magnitude. This suggests that the prominent

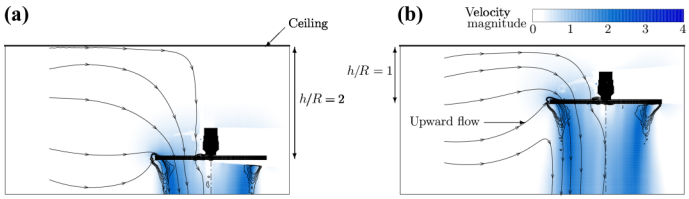

Fig. 7. Streamlines and isolines of radial fluctuating velocities superimposed on contours of velocity magnitude. Flow fields obtained for the $h/R = 2$ (a) and $h/R = 1$ (b) ICE configurations with $\theta = 15°$.

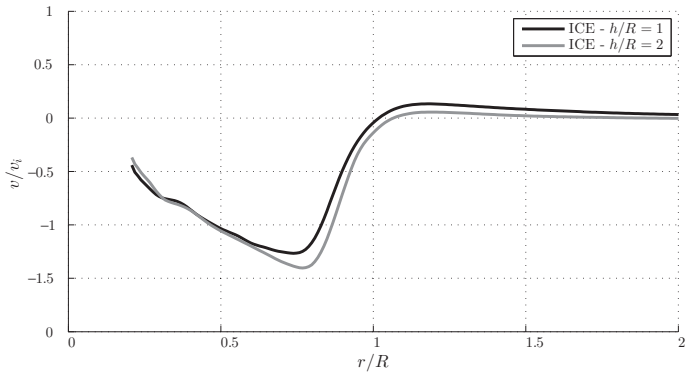

Fig. 8. Nondimensional axial velocity at the rotor disk for the ICE configurations with $\theta = 15°$.

mechanism that leads to an increase in aerodynamic performance is different from that occurring in IGE configurations. Here, as previously mentioned, it can be seen that the rotor feed air comes from aside, and even from beneath of the rotor. As the section between the rotor and the ceiling decreases, the flow increasingly distorts and accelerates toward the rotor. The flow pattern recalls that in a constricted pipe section, which is conducive to Venturi effects. Correlating this to the evolution of $\mathrm{PL_{ICE}/PL_{OGE}}$ as a function of h/R indicates that the rotor is sucked to the ceiling for sufficiently low values of h/R, making it a sudden and severe phenomenon. Besides, although this mechanism differs from that observed in IGE configurations, it should be noted that the reduction in tip vortex strength due to wall proximity is common to both IGE and ICE cases. Overall, three main features can here again be observed: (1) axial velocity along most of the blade span is unchanged, (2) maximum axial velocity is reduced, and (3) upward velocities are induced outside the rotor due to distortion in rotor feed air.

These results show that ICE flight is more beneficial to MAVs endurance than IGE flight is, providing that the MAVs autopilot is sufficiently robust to allow for ICE flight with very low h/R values. Indeed, it should be noted that conversely to IGE configurations, ICE configurations are intrinsically unstable as ceiling suction and rotor thrust act in the same direction. Therefore, there is a significant interest in defining models that contribute to autopilot robustness for ICE flight. As such, Fig. 6 shows that asymptotic models of the form $a \times (h/R)^{-b} + c$, where $b = 1.61$, can provide a reasonable estimate of the evolution of $\mathrm{PL_{ICE}/PL_{OGE}}$ as a function of h/R.

Here again, $\mathrm{PL_{ICE}/PL_{OGE}}$ is roughly independent of DL but depends on the pitch angle θ, as shown in Fig. 9. At this point, it is speculated that the suction force at the ceiling acts normal to the blades such that its contribution to thrust with respect to torque increases as the pitch angle decreases. Hence, $\mathrm{PL_{ICE}}$ at low pitch angles is more sensitive to ceiling suction than $\mathrm{PL_{ICE}}$ at high pitch angles is.

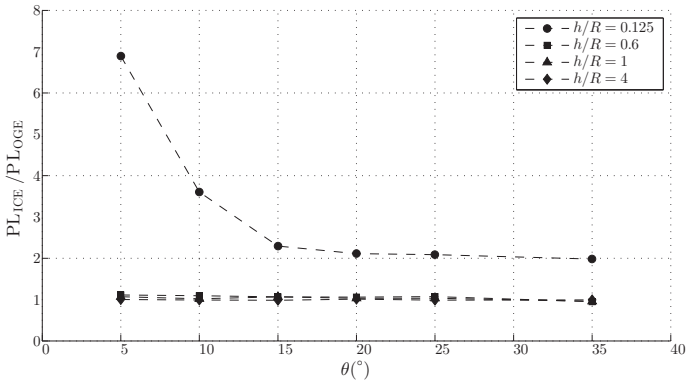

Fig. 9. $\mathrm{PL_{ICE}/PL_{OGE}}$ ratio as a function of pitch angle θ for different h/R values.

Channel effects

In this subsection, we focus on the effects of channel-type confinement on the aerodynamics of microrotors (IChE). Channel configuration results from the combination of IGE and ICE configurations and opens the path toward the study of highly confined configurations typical of indoor flight (e.g., intrusion through vent pipe or underground tunnels). More specifically, in light of previous results, we ask whether IChE aerodynamic performance simply results from the linear combination of IGE and ICE aerodynamic performance or if strong nonlinear coupling tend to generate a completely new scenario.

The distance H between the lower (ground) and upper (ceiling) horizontal walls is introduced.

Figure 10 shows the evolution of the $\mathrm{PL_{IChE}/PL_{OGE}}$ ratio as a function of the rotor to ground distance h/R, at a given DL and for $H/R = 4$, 3, and 2. The evolutions of $\mathrm{PL_{IGE}/PL_{OGE}}$ and $\mathrm{PL_{ICE}/PL_{OGE}}$ are added for ease of comparison. Interestingly, it can be observed that both IGE and ICE data lie upon IChE data for all H/R values, which indicate that the IGE and ICE effects coupling can in a first approach be treated as a linear coupling.

This observation is further highlighted in Fig. 11 for the $H/R = 4$ cases. Overall, it can be seen that the global flow structure above the rotor is roughly similar to that of the ICE case, whereas the global flow structure below the rotor is roughly similar to that of the IGE case. In some way, the rotor acts as an "impermeable frontier" that makes the downstream flow independent of the upstream conditions and vice versa.

Although this statement is reasonably valid for prominent steady flow features, it should be noticed that IChE configurations enhance flow unsteadiness, with higher levels of velocity fluctuations. Unsteady data would be required to determine whether unsteady phenomena are likely to occur at a timescale that is detrimental to MAVs attitude control.

Nonetheless, showing that IChE effects result from the quasi-linear combination of IGE and ICE effects, at least in a mean sense, is conducive to flight robustness in confined environments and provides simple guidelines for the definition of robust autopilot.

Wall effects

We finally address the influence of lateral wall proximity on the aerodynamics of microrotors (IWE). In contrast to previous cases, wall effects break the symmetry of the problem as they influence a limited portion of the rotor disk.

In this particular case, it is observed that the $\mathrm{PL_{IWE}/PL_{OGE}}$ ratio is not significantly affected by wall proximity (and is therefore not shown

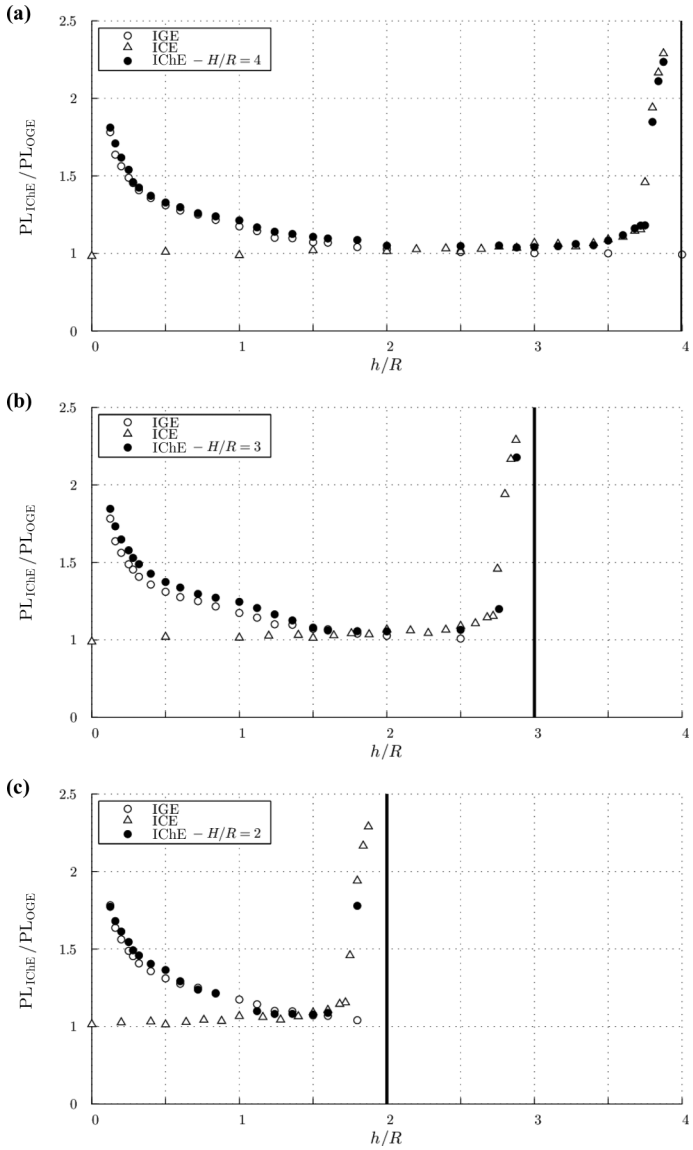

Fig. 10. $\mathrm{PL_{IChE}/PL_{OGE}}$ ratio as a function of the nondimensional rotor-to-ground distance h/R, with $\theta = 15°$. $H/R = 4$ (a), $H/R = 3$ (b), and $H/R = 2$ (c).

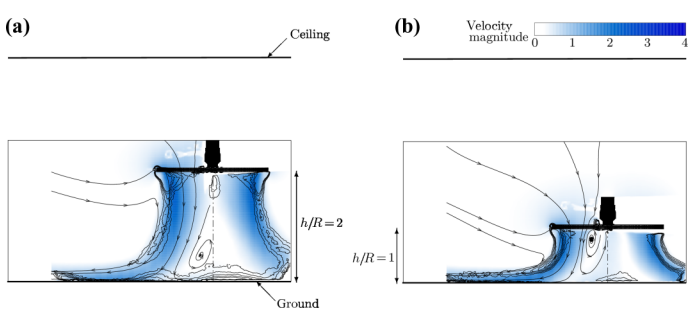

Fig. 11. Streamlines and isolines of radial fluctuating velocities superimposed on contours of velocity magnitude. Flow fields obtained for the $h/R = 2$ (a) and $h/R = 1$ (b) IChE configurations with $\theta = 15°$.

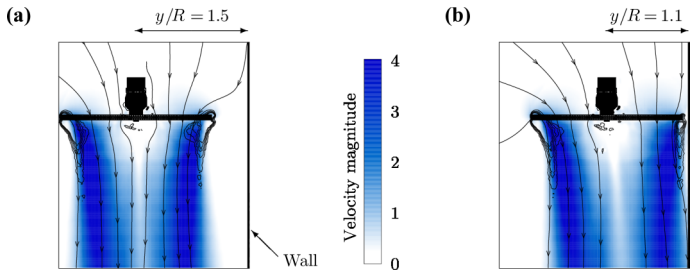

Fig. 12. Streamlines and isolines of radial fluctuating velocities superimposed on contours of velocity magnitude. Flow fields obtained by PIV for the $y/R = 1.5$ (a) and $y/R = 1.1$ (b) IWE configurations with $\theta = 15°$.

here). On the other hand, Fig. 12 shows that the flow structure is modified. As the rotor to wall distance decreases, the rotor jet is sucked toward the wall, which tilts its axis in the counterclockwise direction. In addition, the tip vortex is flattened in the vertical direction and its strength is significantly reduced when approaching the wall. Both wake tilting and changes in tip vortex size and strength naturally induce a lateral force and a rolling moment that is however too weak to be measured here. Flow modifications induced by the proximity of the wall are localized within a small portion of the rotor disk, which makes their influence on aerodynamic loads negligible.

Obviously, this is no more true if the rotor disk is slightly tilted, i.e., if the rotor disk is not strictly perpendicular to the wall and the rotor jet impinges the wall, which is a common feature of advancing rotating wing MAVs. Therefore, for missions in confined environments, there is a significant interest in developing robust attitude control that prevent rotor tilting when performing forward flight toward vertical walls.

Furthermore, additional results have shown that in duct effects, which result from the presence of two parallel lateral walls from both sides of the rotor, do not significantly influence aerodynamic loads either (and is therefore not shown here). Note that such results were obtained for values of y/R as low as 1.1. It is noteworthy to mention that shrouded rotors constitute a limit case where lateral walls are extremely close to the blade tip and affect the whole circumference of the rotor disk. In this regard, previous studies on shrouded rotors (Refs. 25–27) can provide some insights into such extreme wall interactions.

Conclusions

Owing to their small dimensions, MAVs offer the possibility to perform missions of reconnaissance in confined environments. Search and rescue task forces, archeologists, and nuclear security workforces, to name a few, could greatly benefit from MAVs capable of robust indoor flight. In this context, a way to enhance flight robustness is to understand how the rotor of a hovering capable MAV responds to wall proximity in terms of aerodynamics performance.

Toward that end, we conducted experiments on a microrotor hovering in the vicinity of horizontal and vertical walls. By means of force and PIV measurements, we were able to reveal changes in aerodynamic performance due to wall proximity and correlate it with the occurrence of specific flow phenomena. Our results are in line with extensive research on ground effects, showing that aerodynamic performance benefits from ground proximity due to a reduction in induced axial velocity at the rotor disk and reduction in tip vortex strength. It is interesting to note that results obtained for large-scale rotors (reported in Ref. 21) reveal very similar trends, yet with a slightly lower magnitude of the response in thrust to rotor-to-ground distance.

In addition, while ceiling proximity also leads to an enhancement of aerodynamic performance, it is shown that ceiling effects are more severe and sudden than ground effects and can be viewed as a Venturi effect acting above the rotor disk. Furthermore, it can be seen that channel effects can quite surprisingly be considered as a linear combination of both ground and ceiling effects. Conversely, vertical wall proximity does not have a major impact on aerodynamic performance, whether an isolated wall or a duct configuration is considered.

These results help draw guidelines for the definition of efficient autopilots, potentially contributing to indoor flight robustness. However, it should be mentioned that they do not reveal how flow unsteadiness may affect thrust, lateral forces, and pitching and rolling moments, and hence the overall stability of the vehicle. Therefore, to gain further insight into the stability of MAVs operating in confined spaces, future studies should concentrate on flow unsteadiness and extend present results to nonhovering flight phases.

Acknowledgments

The authors would like to thank IDEX Toulouse for partly funding this work. R. Chanton and P. Morel are also greatly acknowledged for test bench design and manufacturing.

References

[1]Mueller, T. J., and DeLaurier, J. D., "Aerodynamics of Small Vehicles," *Annual Review of Fluid Mechanics*, Vol. 35, 2003, pp. 89–111.

[2]Torres, G. E., and Mueller, T. J., "Low Aspect Ratio Aerodynamics at Low Reynolds Numbers," *AIAA Journal*, Vol. 42, (5), 2004, pp. 865–873.

[3]Pines, D. J., and Bohorquez, F., "Challenges Facing Future Micro-Air-Vehicle Development," *Journal of Aircraft*, Vol. 43, (2), 2006, pp. 290–305.

[4]Dickinson, M. H., Lehmann, F. O., and Sane, S. P., "Wing Rotation and the Aerodynamic Basis of Insect Flight," *Science*, Vol. 284, (5422), 1999, pp. 1954–1960.

[5]Platzer, M. F., Jones, K. D., Young, J., and Lai, J. C. S., "Flapping Wing Aerodynamics: Progress and Challenges," *AIAA Journal*, Vol. 46, (9), 2008, pp. 2136–2149.

[6]Shyy, W., Aono, H., Chimakurthi, S. K., Trizila, P., Kang, C. K., Cesnik, C. E. S., and Liu, H., "Recent Progress in Flapping Wing Aerodynamics and Aeroelasticity," *Progress in Aerospace Sciences*, Vol. 46, (7), 2010, pp. 284–327.

[7]Jardin, T., Farcy, A., and David, L., "Three-Dimensional Effects in Hovering Flapping Flight," *Journal of Fluid Mechanics*, Vol. 702, 2012, pp. 102–125.

[8]Ramasamy, M., Lee, T. E., and Leishman, J. G., "Flowfield of a Rotating-Wing Micro Air Vehicle," *Journal of Aircraft*, Vol. 44, (4), 2007, pp. 1236–1244.

[9]Ramasamy, M., Johnson, B., and Leishman, J. G., "Understanding the Aerodynamic Efficiency of a Hovering Microrotor," *Journal of the American Helicopter Society*, Vol. 53, (4), 2008, pp. 412–428.

[10]Bohorquez, F., "Rotor Hover Performance and System Design of an Efficient Coaxial Rotary Wing Micro Air Vehicle," Ph.D. Dissertation, Department of Aerospace Engineering, University of Maryland, College Park, MD, 2007.

[11]Lakshminarayan, V. K., and Baeder, J. D., "Computational Investigation of Microscale Coaxial-Rotor Aerodynamics in Hover," *Journal of Aircraft*, Vol. 47, (3), 2010, pp. 944–950.

[12]Powers, C., Mellinger, D., Kushleyev, A., Kothmann, B., and Kumar, V., "Influence of Aerodynamics and Proximity Effects in Quadrotor Flight," *Springer Tracts in Advanced Robotics*, Vol. 88, 2013, pp. 289–302.

[13]Lee, T. E., Leishman, J. G., and Ramasamy, M., "Fluid Dynamics of Interacting Blade Tip Vortices with a Ground Plane," *Journal of the American Helicopter Society*, **55**, 022005 (2010).

[14]Lakshminarayan, V. K., Kalra, T. S., and Baeder, J. D., "Detailed Computational Investigation of a Hovering Microscale Rotor in Ground Effect," *AIAA Journal*, Vol. 51, (4), 2013, pp. 893–909.

[15]Nathan, N. B., and Green, R. B., "The Flow around a Model Helicopter Main Rotor in Ground Effect," *Experiments in Fluids*, Vol. 52, 2012, pp. 151–166.

[16]Johnson, B., Leishman, J. G., and Sydney, A., "Investigation of Sediment Entrainment Using Dual-Phase, High-Speed Particle Image Velocimetry," *Journal of the American Helicopter Society*, **55**, 042003 (2010).

[17]Sydney, A., and Leishman, J. G., "Time-Resolved Measurements of the Rotor-Induced Particle Flows Produced by a Hovering Rotor," *Journal of the American Helicopter Society*, **59**, 022004 (2014).

[18]Rauleder, J., and Leishman, J. G., "Particle-Fluid Interactions in Rotor-Generated Vortex Flows," *Experiments in Fluids*, Vol. 55, 2014, pp. 1689.

[19]Fradenburgh, E. A., "The Helicopter and the Ground Effect Machine," *Journal of the American Helicopter Society*, Vol. 5, (4), 1960, pp. 24–33.

[20]Curtiss, H. C., Sun, M., Putman, W. F., and Hanker, E. J., "Rotor Aerodynamics in Ground Effect at Low Advance Ratios," *Journal of the American Helicopter Society*, Vol. 29, (1), 1984, pp. 48–55.

[21]Leishman, J. G., *Principles of Helicopter Aerodynamics*, Cambridge University Press, New York, NY, 2000, Chap. 10.

[22]Brown, R. E., and Whitehouse, G. R., "Modelling Rotor Wakes in Ground Effect," *Journal of the American Helicopter Society*, Vol. 49, (3), 2004, pp. 238–249.

[23]Griffiths, D. A., Ananthan, S., and Leishman, J. G., "Predictions of Rotor Performance in Ground Effect Using a Free Vortex Wake Model," *Journal of the American Helicopter Society*, Vol. 50, (4), 2005, pp. 302–314.

[24]Jardin, T., Doué, N., Prothin, S., and Moschetta, J. M., "Numerical Analysis of Pitching Rotor Aerodynamics," *Journal of Fluids and Structures*, Vol. 62, 2016, pp. 172–186.

[25]Pereira, J. L., and Chopra, I., "Hover Tests of Micro Aerial Vehicle Scale Shrouded Rotors, Part I: Performance Characteristics," *Journal of the American Helicopter Society*, **54**, 012001 (2009).

[26]Pereira, J. L., and Chopra, I., "Hover Tests of Micro Aerial Vehicle Scale Shrouded Rotors, Part II: Flow Field Measurements," *Journal of the American Helicopter Society*, **54**, 012002 (2009).

[27]Lakshminarayan, V. K., and Baeder, J. D., "Computational Investigation of Microscale Shrouded Rotor Aerodynamics in Hover," *Journal of the American Helicopter Society*, **56**, 042002 (2011).